European Review for Medical and Pharmacological Sciences 2023; 27: 9401-9412

Alanda *(Ephedra foeminea)* nanoparticles as a modulator of genomic DNA degradation in mice: new inspiration for treating Ehrlich solid tumour-induced kidney and liver toxicity

R.M. ELGHARABAWY[1], E. TOUSSON[2], I.E. EL SAYED[3], A.H. ABD EL-ALEIM[3], M. ELABD[3], D.T. GEBREEL[4], A.S. AHMED[5]

[1]Department of Pharmacology and Toxicology, Faculty of Pharmacy, Tanta University, Tanta, Egypt
[2]Zoology Department, Faculty of Science, Tanta University, Tanta, Egypt
[3]Chemistry Department, Faculty of Science, Menoufia University, Menoufia, Egypt
[4]Medical Equipment Department, Faculty of Allied Medical Sciences, Pharos University in Alexandria, Alexandria, Egypt
[5]Hormones Department, Medical Research and Clinical Studies Institute, National Research Centre, Giza, Egypt

Abstract. – OBJECTIVE: The limitations faced by conventional drug delivery systems are being overcome through the use of rapidly evolving cancer nanotherapeutics. Determining the manner in which the Ehrlich solid tumor (EST) is impacted by the new bioactive Alanda-loaded flax seed gum nanoparticles (Alanda NPs) functioning as an anti-carcinogenic agent represents the research objective of this paper.

MATERIALS AND METHODS: Identification of the functional groups, surface morphology, particle size, and zeta potential were among the characterizations and preparations made for the prepared nanoparticles. A Control group, a Flax Seed Gum group, a raw Alanda group, an Alanda NPs group, an EST group, and an induced EST treated with Alanda NPs group comprised the six groups respectively which the 60 female mice were separated into in this *in vivo* study.

RESULTS: Toxicity assessments for kidneys and liver were performed alongside the detection of total genomic DNA degradation. The zeta potential and the particle sizes for Alanda NPs were -25.60±0.38 mv and 40±0.28 nm, respectively, where the latter demonstrated a monodisperse spherical shape, per the findings. The use of Alanda NPs to treat EST was found to alleviate the DNA damage, apoptosis, and renal and hepatic toxicity that EST induces. Additionally, the activation of oxidative stress and apoptosis causing the renal and hepatic toxicity induced by EST is counteracted by the scavenging of free radicals by the Alanda NPs.

CONCLUSIONS: A high degree of safety for effective cancer treatment was displayed by the newly developed oral nanoparticles while also demonstrating strong potential *in vivo*.

Key Words:
Apoptosis, Renal and hepatic toxicity, Ehrlich solid tumour, DNA damage, *Ephedra foeminea*.

Introduction

Cancer occurs when abnormal cells grow uncontrollably and invade surrounding tissues. Tousson et al[1-3] noted that by instigating apoptosis, such abnormal and lethal growth cells are killed in the most common cancer treatments – radiation and chemotherapy. As shown by many studies[4-6], the analysis of antineoplastic impacts of multiple substance compounds is enabled by the use of the Ehrlich tumor as a transplantable growth model. According to Abdelbasset et al[7] and others[8,9], the second most common type of tumor internationally is breast cancer, which is the most frequent type of cancer in women.

Studies outline[10-12] that a spontaneous murine mammary adenocarcinoma similar to breast cancer was the initial categorization made for the EST. Abd Eldaim et al[13-15] note that oxidative stress and toxicity are ways EST negatively impacts the liver and kidney tissue.

Notably, Elgharabawy et al[16] state that possible cancer treatments intriguingly include plants, among many other sources of compounds. Several studies[17-20] show that synthetic antioxidants, endogenous antioxidants, and elevated oxidative damage are probable outcomes of the strong correlation between cancer and mortality and morbidity of liver and kidney diseases.

Corresponding Author: Rehab Mohamed Elgharabawy, MD; e-mail: drrehab200932@yahoo.com

Mighri et al[21] and Chouikh[22] identify the origins of the *Ephedra foeminea*, a low stalky Eurasian shrub from the Ephedraceae lineage, as native to the entire southeast of the Mediterranean and northern Israel, otherwise known in Arabic as Alanda. It has been used for at least 5,000 years by the Chinese, thereby representing one of the oldest drugs in the world. Some researchers[23,24] note that alkaloids of the ephedrine E-type, that function as sympathomimetics, reside within the Alanda. The receptor binding and enantiomeric form features alongside the individual E alkaloid type determine the toxicological and pharmacological effects. As outlined by many studies[25-28], weight reduction, anti-proliferative, anti-asthmatic, antioxidant, hypoglycemic, anti-microbial, and anti-inflammatory effects are among the activities exhibited by the Ephedra. Danciu et al[29] observe that Ephedrine binds to adrenergic receptors and resultantly causes notable effects on the central nervous system while elevating blood pressure and stimulating the heart rate. In the context of treating cancer, there is sparse knowledge on the use of Alanda. Notably, Mendelovich et al[30] state that metastasis and cancer cell invasiveness are correlated to the impact of Alanda on gene expression and cell cytoskeleton, thereby reflecting the potential harm of using Alanda to treat cancer. Severe neurological and cardiovascular system toxicity has also been linked to ephedrine alkaloid components that reside within Alanda. As Jaradat et al[31] highlight, the USA chose to ban the use of the plant after severe issues causing death and toxic effects occurred.

The development of new drug carrier designs for particular applications could advance significantly *via* natural polymeric-based nanomaterials. Moreover, as Zhao et al[32] observe, substantial immunological responses with optimal biological safety can be induced by such nanoparticles that possess therapeutic characteristics. A natural heterogeneous polysaccharide is found in *Linium usitatissimum* L., otherwise known as Flax seed gum. The presence of groups that can be altered for functionalization and biocompatibility are among the most salient advantages of utilizing polysaccharides. Mittal et al[33] determine that risks linked to toxic drugs are mitigated by Flax seed gum which is also utilized more commonly as stabilizers, suspending agents, carriers, binders, and disintegrating agents.

Low therapeutic indices, deficient water solubility, nonspecific targeting and bio-distribution, and poor oral bioavailability are among the restrictions of conventional drug delivery systems that the application of cancer nanotherapeutics resolves. The circulation time in the bloodstream of these nanoparticles is augmented *via* nanoparticles with optimally designed surface characteristics and size, thereby enhancing the bio-distribution of cancer drugs. Examining how the Ehrlich solid tumor and its effects on the kidney and liver, such as DNA damage, apoptosis, and toxicity, are impacted by Alanda in nano form comprises the research objective of this paper.

Materials and Methods

Extraction and Purification of Flax Seed Gum

A local market served to provision the flax seeds. The seeds of *Linum usitatissimum* were used to extract the Flax seed gum *via* the aqueous method, with modifications noted by Neeraj et al[34]. The seeds were stirred by a magnetic stirrer for two hours at 80°C at 1,200 rpm, following the soaking of the dried seeds in 10 folds of distilled water. A muslin cloth was used to filter the resultant viscous solution, which then led to centrifugation for 20 minutes at 4,000 rpm. Lastly, a lyophilizer was used to dry the cream-colored precipitates of gum that were separated by filtration.

Extraction and Purification of Ephedra

A mechanical miller was utilized to grind five grams of a specifically chosen aerial portion of the plant. The produced powder had 50 ml of 5% vinegar, otherwise called acetic acid, incorporated into it. The sample was then incubated overnight at 30°C with automatic shaking at 160 rpm. Next, the supernatant was decanted after the mixture was centrifuged at 3,000 rpm for 20 minutes. Then, incubation for 30 minutes at room temperature occurred after the dried sample had 20 ml of vinegar added to it. In line with previous studies[30,35], the mixture was homogenized by vortex after 10 ml of distilled water was added and then a syringe 0.45 µm Teflon filter was used to filter the solution.

Preparation of Ephedra-loaded Nanoparticles

In accordance with Madani et al[36], the modified oil in water (O/W) single emulsion solvent evaporation method was used to prepare the nanoparticles. A homogenous solution was at-

tained by using a magnetic stirrer for four hours at 40°C to stir the surfactant arising from the aqueous phase consisting of 10% concentration (90 ml) of Flax seed gum. The aqueous phases subjected to non-stop magnetic stirring at room temperature for 30 minutes had the organic phase comprising 10 ml of Ephedra extraction added to it in order to generate O/W emulsion type. Then, a sonication water bath was used for 15 minutes to diminish the size of the nanoparticles, thereby sonicating the emulsion. The organic solvent was evaporated by using a magnetic stirrer at room temperature for three hours at 1,200 rpm to stir the formed O/W emulsion. Ultracentrifugation at room temperature for 15 minutes at 4,000 rpm was used to recover the nanoparticles that were then washed with deionized water twice.

Characterization of Nanoparticles

Scanning electron microscopy (SEM)

Scanning electron microscopy was used to observe the surface morphology and diameter of the Ephedra nanoparticles. The Sem Afore (4.01 demo, JEOI, Finland) software was used to randomly choose 30 nanoparticles and identify the diameter of the nanoparticles.

Transmission electron microscopy (TEM (

A transmission electron microscope (JEOL JEM-1400 120kV; Jeol Ltd., Tokyo, Japan) was used to identify the morphology and size of the Ephedra-loaded nanoparticles.

Fourier transform infrared spectroscopy (FTIR)

The potential interactions of Flax seed gum and Ephedra were analyzed by monitoring the FTIR spectra for Ephedra-loaded nanoparticles and the raw material of Ephedra.

Zeta Potential

The degree of stability in aqueous nanoparticle dispersion is regulated *via* the zeta potential that represents a surface charge measurement. Zeta potential values, whether negative or positive, should be high in order to avert aggregation and ensure particle stability. The Zetasizer Nano ZS (Malvern Instruments, Malvern, Worcestershire, UK) was used to evaluate the zeta potential.

Animals

The animal house colony Egypt vaccine company was the source of the 40 Swiss albino female mice, weighing between 20 and 25 g, procured for this paper. Relative stickiness conditions consisting of 12 hours of light and dim cycles respectively, alongside room temperatures between 22 and 25°C housed the mice that were all randomized.

Animal groups and experimental designs

The mice were separated into six groups (Gp1-Gp6) as demonstrated below:

- Gp1: the Control Gp of untreated mice.
- Gp2: The mice orally received 25 mg/kg bw/2day of Flax seed gum by stomach tube for roughly 15 days in this Flax Seed Gum Gp (FSG).
- Gp3: The mice orally received 25 mg/kg bw/2day of the powder from the areal parts of the Alanda *via* stomach tube for roughly 15 days in the raw Alanda Gp (Alanda).
- Gp4: The mice orally received 25 mg/kg bw/2day of Alanda NPs *via* stomach tube for roughly 15 days in the Alanda nanoparticles Gp (Alanda NPs).
- Gp5: In line with Aldubayan et al[10], the mice were infused hypodermically with roughly 2,500,000 cells of EAC per mouse debilitated in buffer saline to start EST in the Ehrlich solid tumor Gp (EST) mice.
- Gp6: Treatment with only Alanda nanoparticles (Alanda NPs) for 15 days follows the hypodermic infusion of 2,500,000 cells of EAC per mouse to commence the tumor (EST), which is then left for roughly 15 days in the EST+Alanda NPs Gp.

Blood and Serum Samples

Clotting was enabled by the exclusion of anticoagulant substances in the sterile and dry tube, which aseptically collected the blood samples *via* venipuncture. Centrifugation at 3,000 rpm for 10 minutes followed clot formation, which occurred after the blood samples were left alone at 4°C for 30 minutes. Up until assessments of certain blood parameters were made, temperatures of -18°C were used to store the collected serum.

Evaluation of Serum Liver Function Tests

In line with Reitman and Frankel[37] the serums aspartate transaminase (AST) and alanine transaminase (ALT) were assessed. The estimation of alkaline phosphatase and albumin concentration activity in sera followed the example of separate academic works[38,39]. Conversely, the evaluation of the serum total protein level adhered to the work of another research paper[40].

Electrolytes and Kidney Functions Biomarker

The estimation of urea occurred in accordance with a certain investigation[41]. Diamond, based in Egypt, provided a commercial kit that was used to evaluate the creatinine concentration in serum. Bowers and Wong[41] presented the technique used in this paper to estimate creatinine levels. The use of commercial kits (Sensa core electrolyte, Bengaluru, Karnataka, India) enabled the estimation of the levels of serum electrolytes, such as chloride, sodium, potassium, and calcium ions[42].

Detection of Total Genomic DNA Degradation

As demonstrated in another academic work, the salting out extraction technique was used to detect DNA degradation *via* agarose gel electrophoresis after Labarca and Paigen[43] The ImageJ software, as an average optical density value, enabled the assessment of the intensity of DNA fragmentation.

Histopathological Evaluation

Processing for paraffin sectioning followed the immediate incorporation of 10% buffer-neutral formalin solution for one to two days to the kidney and liver tissues. In line with Tousson[44], the histopathological assessment was enabled by staining the sections with hematoxylin and eosin (H&E).

Immunohistochemical Detection of P53 Immunoreactivities

The use of the Avidin Biotin Complex (ABC) enabled detection in the kidney and liver sections of the expression of apoptotic P53 immunoreactivities (P53-ir)[2].

Immunohistochemical Detection of Bcl2 Immunoreactivities

Similarly, the use of ABC enabled detection in the kidney and liver sections of the expression of anti-apoptotic Bcl2 immunoreactivities (Bcl2-ir)[2].

Statistical Analysis

An unpaired *t*-test to evaluate the salient variances among treatment groups enabled the undertaking of statistical analysis where data were expressed as average values ± SE. The threshold for the biochemical data representing the criterion of statistically significant data was 0.05. The SPSS statistical version 21 software package (IBM Corp., Armonk, NY, USA) was used to conduct all statistical analyses.

Results

Scanning Electron Microscopy (SEM)

The surface morphology and shape of the Ephedra nanoparticles loaded with flax seed extract were validated *via* the use of SEM. The shape of the particles was revealed to be entirely spherical, as demonstrated by the SEM image in Figure 1A. The amorphous and smooth nature of natural polymers was implicated by the SEM scans.

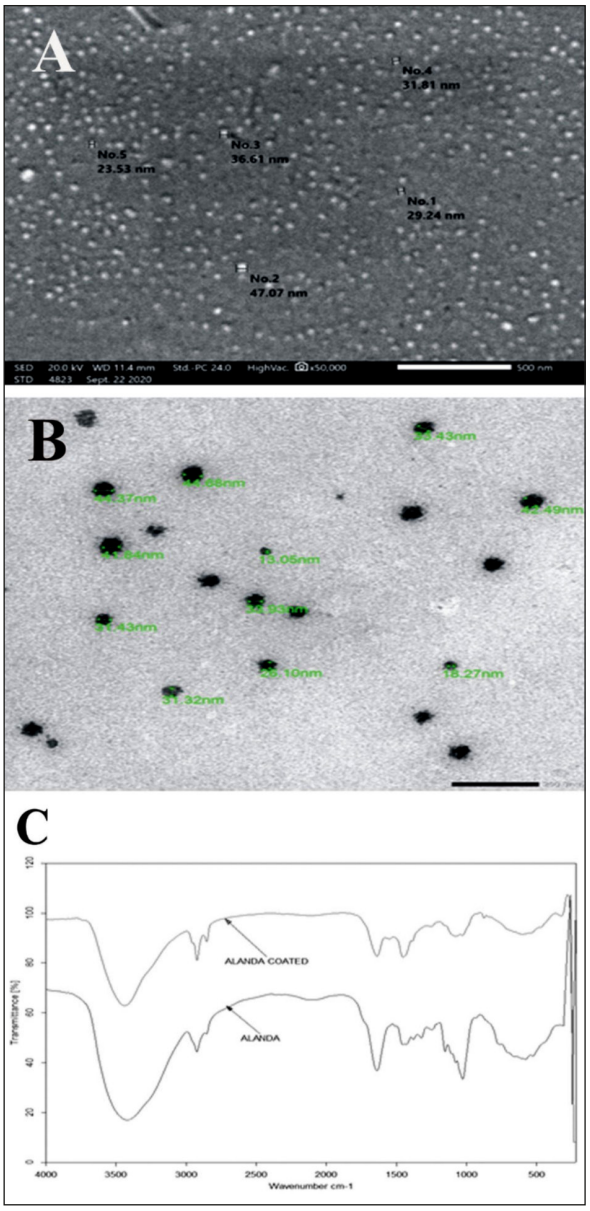

Figure 1. A-B, Scanning Electron Microscopy (SEM) and Transmission electron microscopy (TEM) images of the Ephedra-coated nanoparticles. **C**, Fourier transform infrared spectroscopy (FTIR) spectra at wavenumber of 4,000 to 400 cm-1 of Ephedra and Ephedra nanoparticles coated with flax seeds extract.

Transmission Electron Microscopy (TEM)

Figure 1B demonstrates that TEM image where very monodisperse nanoparticles are generated without defects, validating the synthesis of high quality. Similarly, the amorphous and spherical nature of the nanoparticles was revealed. An average size of 40 nm was observed in the particles. The generation of an amorphous polymer-drug structure is indicated, as per prior evidence.

Fourier Transform Infrared Spectroscopy (FTIR)

The potential alterations in the structure following the addition of flax seed extract are assessed after the chemical bonding and functional groups of the prepared Ephedra nanoparticles are determined *via* the FTIR. The stretching of the CH- groups of alkanes and the hydroxyl (-OH) groups of aliphatic alcohol demonstrated sharp peaks at 2,929 cm^{-1} and 3,430 cm^{-1}, respectively, as per Figure 1C that shows the formulation of Ephedra-coated particles and the observed characteristic peaks of the Ephedra. The stretching of the carbonyl group C=O and PO_2 caused the observed peaks of 1,037 cm^{-1} and 1,621 cm^{-1}. Consequently, when the nanoparticles had flax seed extract added to them, no alteration occurred in the positioning of such peaks. Thus, as demonstrated in Figure 1C, the absence of interactions between flax seed extracts and Ephedra is proven by the nearly equivalent spectra displayed by the Ephedra nanoparticles and Ephedra materials.

Zeta Potential

An anionic nature was observed in the Ephedra nanoparticles, as suggested by their negative zeta potential of -25 mV. Neeraj et al[34] note that increased bio-adhesive strength is demonstrated by polyanions, in comparison to polycations. The stability of the Flax seed gum loaded with Ephedra was guaranteed by the high zeta potential value.

Kidney Functions and Electrolytes Biomarker

Upon comparing the control mice, a substantial reduction of Ca++ and Na+ ($p<0.05$) in EST was observed, while a substantial rise in Cl- and K+ ($p<0.05$) was witnessed in the creatinine and serum levels, as portrayed in Table I. Nevertheless, upon comparison with the EST group, EST treated with Alanda demonstrated a substantial rise in Ca++ and Na+ levels ($p<0.05$) while a substantial reduction in Cl- and K+ levels ($p<0.05$) of creatinine and urea were also witnessed.

Liver Functions Biomarker

Upon comparing the control mice, a substantial reduction of the albumin and total protein ($p<0.05$) was observed in EST, while a substantial rise ($p<0.05$) in the serum alkaline phosphatase (ALP), Glutamic-oxaloacetic transaminase (GOT), and Glutamic-pyruvic transaminase (GPT) concurrently was witnessed (Table II). Nevertheless, upon comparison with the EST group, EST treated with Alanda exhibited a substantial rise in albumin ($p<0.05$) while also demonstrating a substantial reduction ($p<0.05$) in the total protein, ALP, GOT, and GPT (Table II).

Total Genomic Degraded DNA in the Kidney and Liver

The total genomic DNA degradation in the kidney and liver is portrayed in Figure 2. Compared with FSG (KG1, KG2, LG1, and LG2) and the negative control, the sparse fragmentation witnessed in the Alanda NPs group (KG4 and LG4) can be ignored. Conversely, serious necrosis (smear shape) was linked to a late stage of apoptosis witnessed in the small amount of DNA damage provoked by the EST and Alanda groups (KG3, KG5, LG3, and LG5). Nevertheless, EST-induced DNA damage to

Table I. Changes in serum electrolytes and kidney function levels.

	Urea (gm/dl)	Creatinine (gm/dl)	Na+ (mmol/l)	K+ (mmol/l)	Ca++ (mmol/l)	Cl- (mmol/l)
Control	$26.75^{\#}$±1.38	$0.52^{\#}$±0.18	$136.6^{\#}$±8.8	$4.19^{\#}$±0.24	$1.12^{\#}$±0.01	$101.5^{\#}$±8.9
FSG	$26.15^{\#}$±1.62	$0.55^{\#}$±0.13	$137.0^{\#}$±7.4	$4.22^{\#}$±0.31	$1.09^{\#}$±0.09	$107.0^{\#}$±7.5
Alanda	$33.0^{\#}$*±1.15	$0.59^{\#}$±0.22	$131.0^{\#}$*±6.6	$4.59^{\#}$*±0.30	$0.91^{\#}$*±0.03	$109.5^{\#}$*±8.5
Alanda Nps	$25.25^{\#}$±1.55	$0.40^{\#}$±0.03	$135.5^{\#}$±9.6	$4.74^{\#}$±0.22	$1.06^{\#}$±0.03	$100.8^{\#}$±6.6
EST	54.5*±2.96	0.98*±0.06	124.5*±7.1	6.06±0.54	0.89*±0.01	116.4*±8.2
EST+ Alanda Nps	$27.0^{\#}$±0.91	$0.45^{\#}$±0.02	$134.5^{\#}$±9.7	$4.50^{\#}$*±0.29	$1.01^{\#}$±0.01	$107.8^{\#}$*±6.7

Data are expressed as mean±S.E.M. (*) and (#) significant difference compared to control and Ehrlich solid tumor (EST) at $p<0.05$ respectively.

Table II. Changes in serum liver enzymes (GPT, GOT, ALP, total protein, albumin) levels.

	GPT (U/l)	GOT (U/l)	Alb (gm/dl)	ALP (U/l)	T. protein (gm/dl)
Control	44.5$^{\#}$±1.44	141.0$^{\#}$±3.81	4.38$^{\#}$±0.03	188.3$^{\#}$±4.6	5.92$^{\#}$±0.12
FSG	45.1$^{\#}$±1.60	147.0$^{\#}$±6.44	4.21$^{\#}$±0.18	192.5$^{\#}$±9.07	5.66$^{\#}$±0.38
Alanda	60.26$^{\#}$*± 4.25	171.5$^{\#}$*±9.39	3.86$^{\#}$*±0.35	229.0$^{\#}$*±12.5	5.12$^{\#}$*±0.33
Alanda Nps	42.0$^{\#}$±1.581	139.3$^{\#}$±4.07	4.12$^{\#}$±0.06	204.8$^{\#}$±5.27	5.77$^{\#}$±0.04
EST	82.3*±3.09	295.0*±4.42	3.43*±0.09	483.3*±16.5	4.70*±0.08
EST+ Alanda Nps	59.3$^{\#}$*± 3.64	168.0$^{\#}$*±6.28	4.23$^{\#}$±0.45	208.5$^{\#}$±9.5	5.23$^{\#}$*±0.08

Ehrlich solid tumor (EST); Flax Seed Gum (FSG); alkaline phosphatase (ALP).
Data are expressed as mean ± S.E.M. (*) and ($^{\#}$) significant differences compared to control and EST, respectively, at $p<0.05$.

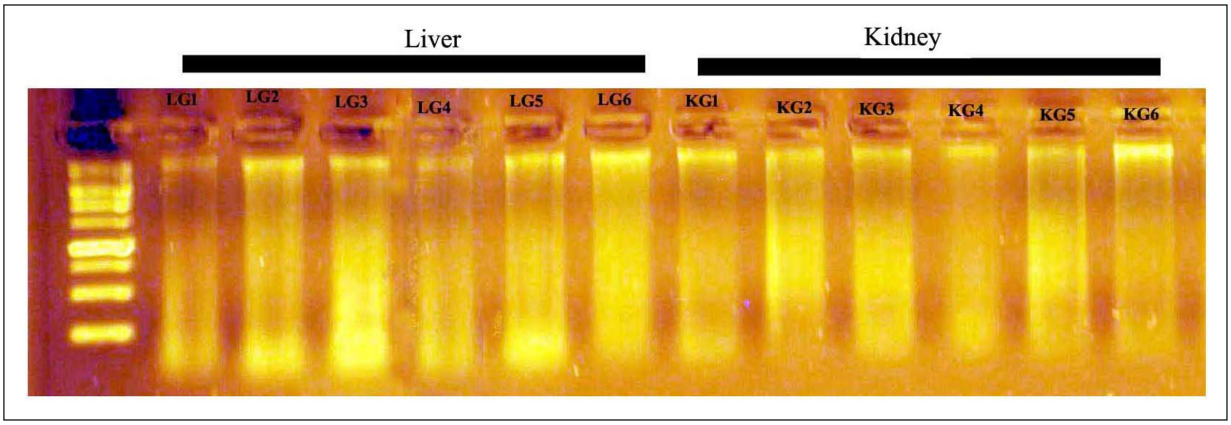

Figure 2. Stained agarose gel of genomic degraded DNA of liver (L) and kidney (K) demonstrating apoptotic and necrotic cell deaths induced by EST. G1, control; G2, FSG; G3, Alanda; G4, Alanda NPs; G5, EST; G6, treated EST with Alanda NPs.

the tissues of the kidney and liver (KG6 and LG6) was mitigated by the protective impact of Alanda NPs within the EST group treated with Alanda NPs.

Kidney Histopathology Findings

As demonstrated in Figures 3A-D, standard histological structures were observed in the medullary and cortical areas of the renal and glomeruli tubules within the Alanda NPs group (G4), FSG (G2), and control group (G1). Conversely, Figure 4C portrays atrophy in the tubular and glomeruli cells and moderate degeneration in the Alanda (G3) kidney sections. Figure 3E demonstrates atrophy in tubular cells, moderate degeneration, and marked inflammatory cellular infiltration in the kidney sections of the EST group (G3), also displaying variable histological alterations in certain portions of the urinary tubules and glomeruli. Figure 3F illustrates mild degeneration of the urinary and moderate atrophy of the tubular cells within the kidney sections of the EST treated with Alanda NPs group (G6).

Histological Alterations in the Liver

As shown in Figures 3A-B and 3D focusing on liver sections, a network extending from a central vein to the edges of the hepatic lobules where the portal tracts appeared form due to the radiating cords of hepatocytes configured in the form of strands or anastomosing cords that surround the normal central vein, thereby demonstrating a standard histological pattern in the Alanda NPs group (G4), FSG (G2), and control group (G1). Contrastingly, Figure 3C portrays severe inflammatory cell infiltration and tissue degeneration within the liver sections of the mice treated with Alanda (G3). As demonstrated by Figure 3E, congestion in the portal and central veins or marked dilation, cellular infiltrations, and marked atrophied vacuolar degeneration of hepatocytes were observed in the EST group (G5). In addition, Figure 3F displays the marked diffuse necrosis of hepatic tissue, moderate inflammatory cells, and moderate cytoplasmic vacuolization of hepatocytes within the liver sections of the EST treated with Alanda NPs (G6).

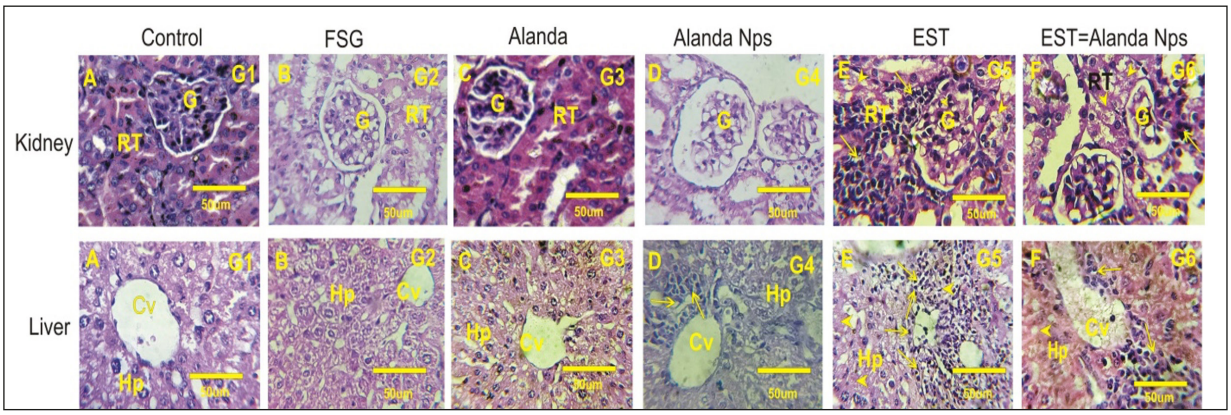

Figure 3. Photomicrographs of mice kidney and liver sections in the different experimental groups stained with Haematoxylin & Eosin. **A-B**, **D**, Liver sections in control (G1), FSG (G2), and treated mice Alanda NPs (G4) groups revealed normal histological pattern with normal central vein is surrounded by radiating cords of hepatocytes (Hp) and normal central vein (Cv). **C**, Liver sections in Alanda (G3) revealed extensive degeneration of tissue and inflammatory cells infiltrations (arrows). **E**, Liver section in EST (G5) revealed degeneration of hepatocytes (arrow heads) and marked inflammatory cells infiltrations (arrows). **F**, Liver sections in treated EST with Alanda NPs (G6) revealed a moderate diffuse necrosis of hepatic tissue (arrow heads) and moderate inflammatory cells infiltrations (arrows) (Magnification power is 25). **A-B**, **D**, Kidney sections in control (G1), FSG (G2) and treated mice Alanda NPs (G4) groups revealed normal histological structures of the glomruli (G) and renal tubules (Tb). E: Kidney sections in EST (G5) revealed marked inflammatory cellular infiltration (arrows) and moderate degenerative and, atrophy in tubular cells tublar cells marked degenerated (arrow heads). F: Kidney sections in treated EST with Alanda NPs (G6) group revealed a moderate atrophy in tubular cells, with mild degenerated urinary (Magnification power is 50 um).

Bcl2 Immunohistochemical Alterations in the Liver

Figures 4 and 5 portray the distribution and detection of Bcl2 immunoreactivity (Bcl2-ir) in liver sections of the distinct groups. A significantly positive reaction for Bcl2-ir (grade 5) in hepatocytes was observed within the liver sections of the Alanda NPs, FSG, and control groups. The

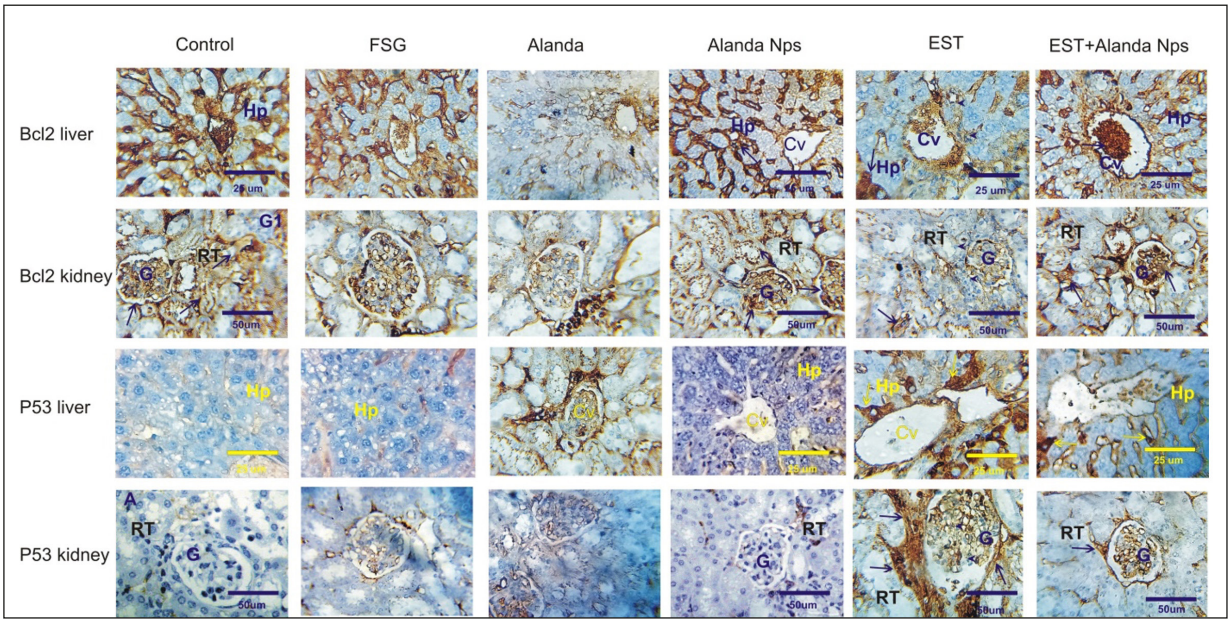

Figure 4. Immunohistochemical localization of anti-apoptotic Bcl2 and apoptotic P53- dependent pathway in liver and kidney sections in different groups, indicated a marked downregulation of Bcl2 expression in EST and elevation in P53 on liver and kidney, while and elevation of Bcl2 expression and depletion in P53 in EST+Alanda NPs on liver and kidney (Magnification power is 25 and 50 um respectively).

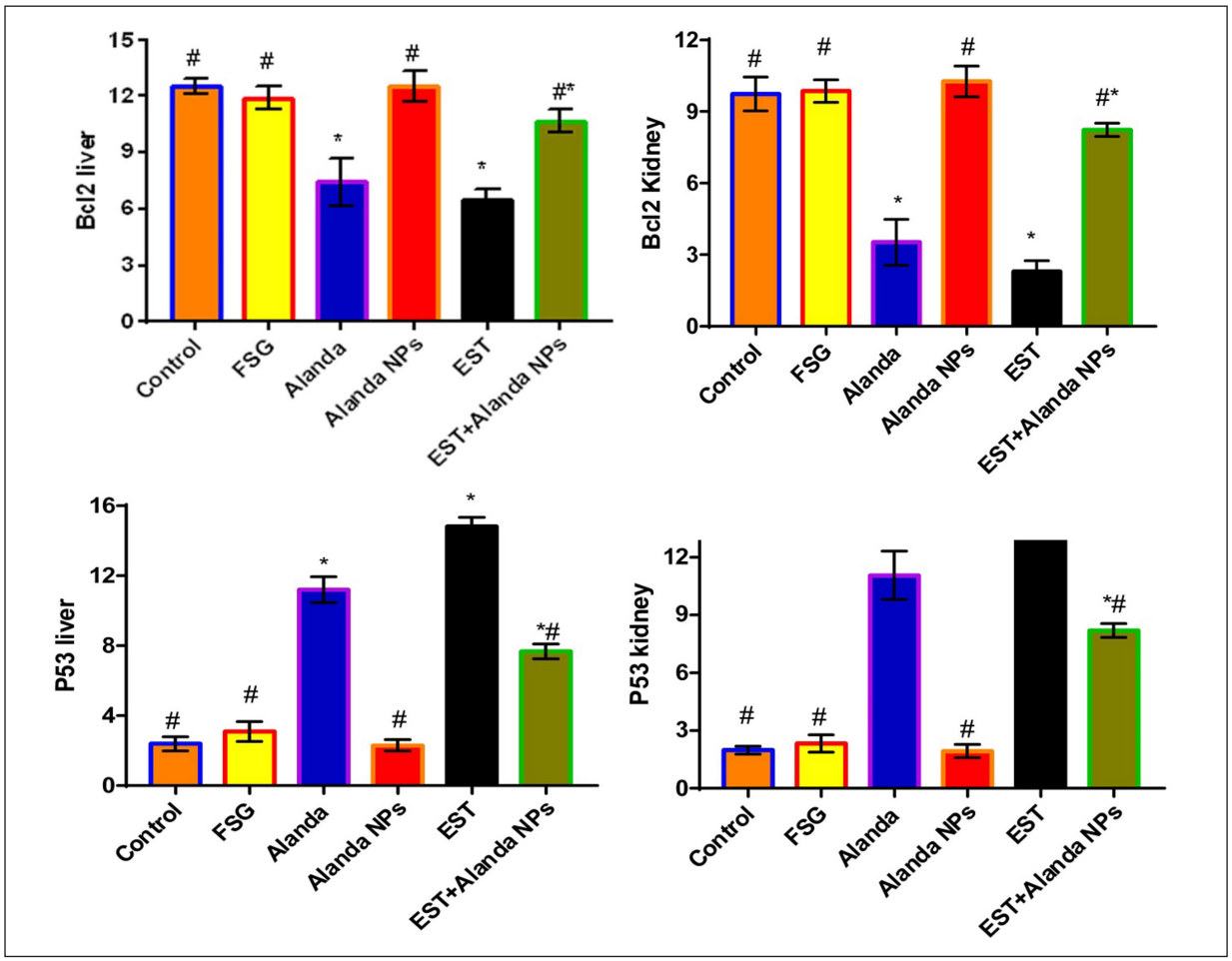

Figure 5. Data represent the expression level of Bcl2 and P53 in liver and kidney tissues in different experimental groups. Columns with different signs are significantly different ($p<.05$) Where (*) and (#) significant difference compared to control and EST respectively.

liver sections in the Alanda group displayed a moderately positive reaction for Bcl2-ir (grade 3). In addition, the liver sections in the EST group displayed mildly positive reactions for Bcl2-ir (grade 2). Upon comparison with the control group, a substantial reduction in the intensity of Bcl2-ir was observed in the liver sections of the EST group. Contrastingly, moderately positive reactions for Bcl2-ir (grade 4) were witnessed in the liver sections of the EST treated with the Alanda NPs group.

Bcl2 Immunohistochemical Alterations in the Kidney

Figures 4 and 5 show the distribution and detection of Bcl2 immunoreactivity (Bcl2-ir) in kidney sections of the distinct groups. A significantly positive reaction for Bcl2-ir (grade 5) in renal and glomeruli tubules within the medullary and cortical areas was observed within the liver sections of the Alanda NPs, FSG, and control groups. The kidney sections in the EST group displayed a faintly positive reaction for Bcl2-ir (grade 1), while the Alanda group displayed a mildly positive reaction for Bcl2-ir (grade 2). Upon comparison with the control group, a substantial rise in the intensity of Bcl2-ir was observed in the liver sections of the EST group. Nonetheless, mildly positive reactions for Bcl2-ir (grade 3) were witnessed in the kidney sections of the EST treated with the Alanda NPs group.

P53 Immunohistochemical Alterations in the Liver

Figures 4 and 5 illustrate the distribution and detection of P53 immunoreactivity (P53-ir) in liver sections of the distinct groups. A faintly positive reaction for P53-ir (grade 2) in the hepatocytes was

observed within the liver sections of the Alanda NPs, FSG, and control groups. The liver sections in the Alanda group displayed a moderately positive reaction for P53-ir (grade 4), whereas the liver sections of the EST group displayed a strongly positive reaction for P53-ir (grade 5). Upon comparison with the control group, a substantial rise in the intensity of P53-ir was observed in the liver sections of the EST group. Nonetheless, mild to moderate positive reactions for P53-ir (grade 3) were witnessed in the liver sections of the EST treated with the Alanda NPs group.

P53 Immunohistochemical Alterations in the Kidney

Figures 4 and 5 display the distribution and detection of P53 immunoreactivity (P53-ir) in kidney sections of the distinct groups. A faintly positive reaction for P53-ir (grade 1) in the renal and glomeruli tubules within the medullary and cortical areas was observed within the kidney sections of the Alanda NPs, FSG, and control groups. The kidney sections in the Alanda group displayed a moderately positive reaction for P53-ir (grade 2), whereas the kidney sections of the EST group displayed a strongly positive reaction for P53-ir (grade 3). Upon comparison with the control group, a substantial rise in the intensity of P53-ir was observed in the kidney sections of the EST group. Nevertheless, mildly positive reactions for P53-ir (grade 2) were witnessed in the liver sections of the EST treated with the Alanda NPs group.

Discussion

As Aldubayan et al[10] and Kabel et al[45] observe, the increased sensitivity to chemotherapy and the rapid advancement rate of Ehrlich carcinoma make it almost an exact equivalent to human cancers. The development of tumors in animals significantly impacts organ function. The exhaustion of total albumin and protein levels, alongside the rise in ALP, AST, and ALT activities, characterize the liver dysfunction provoked by the Ehrlich solid tumor, as this paper shows. Nevertheless, such alterations to the liver functions were positively mitigated when the Est was treated with Alanda NPs. It is possible that a reduction in the leakage of enzymes into blood circulation occurs due to the stabilization of the hepatic cellular membrane damage as a result of rises in ALP, ALT, and AST levels in sera, which validate the capability of such substances in safeguarding the hepatocyte against membrane fragility. The change of hepatic enzymes and tissue architectures characterize the EST-induced hepatoxicity witnessed in separate academic works, thereby corroborating the findings of this study[10,14]. Additionally, the exhaustion of albumin and total protein levels induced by EAC is also reported in another research paper[46]. Khali et al[27] note that the antioxidant and scavenging properties, in tandem with the stimulating impact on antioxidative defense systems of Alanda NPs, aid the hepatic protective effect of the substance, which decreases the activities of ALP, ALT, and AST upon its incorporation.

A renal tissue injury induced by EST could be the cause of the diminished level of sodium and calcium ions and the heightened levels of chloride, urea, creatinine, and potassium ions, thereby reflecting the changes to kidney functions induced by EST. Conversely, these changes in electrolytes and kidney functions are mitigated when EST is treated with Alanda NPs. Waste products are excreted as the kidney loses efficiency upon increased levels of creatinine and urea, causing reduced glomerular filtration rates. As Salama et al[47] observe, a rupture in the integrity of the cell membrane, loss of function, and cellular leakage in the kidney are indicated by the mentioned biomarkers. Moreover, increased levels of creatinine and urea were found to be the outlet through which EST provokes renal dysfunction in another study[13], thus corroborating the findings of this study. Similarly, reductions in sodium ions and heightened levels of chloride, creatinine, urea, and potassium ions were found to cause substantial alterations in renal functionality and kidney injury within the Ehrlich ascites tumor, as per another academic work that reflects the results of this paper[4].

Chromosomal aberrations, mutations, and DNA damage occurred due to the aggregation of reactive oxygen species (ROS) within women's bodies in tandem with breast cancer development, as per another research paper reflecting the results of this academic work[8]. As Abd Eldaim et al[13,14] observe, ROS plays a significant role in provoking tissue damage after applying oxidative stress that demolishes cellular homeostasis once EST is induced, resulting in changes to the kidney and liver structure, per the results of this paper. Given that the kidney section of the EST group displayed renal toxicity in the form of atrophy of glomeruli and tubular cells as well as marked degeneration, the findings of the im-

munohistochemical and histopathological evaluation of kidney tissues were corroborated by the biochemical findings of this paper.

By decreasing the severe effects of EST on renal and hepatic tissue architecture, DNA damage, and serum levels of kidney and liver function, the results of this paper were presented. Furthermore, the Bcl2 expressions in renal and hepatic tissues were reduced, while the P53 expressions in these tissues were elevated. Khalil et al[27] note that antioxidant activities may be the source of the beneficial effects of Alanda NPs. The mitochondrial destruction and accumulation of inflammatory cells caused by the migration and proliferation of tumor cells are attributed to the effect of the infiltration of Ehrlich tumor cells in internal organs in an academic work[5]. While leaving cell replication multiplication untouched, apoptosis is a significant procedure that maintains cell numbers at optimal levels. Al-Rasheed et al[48] and Alapati et al[49] state that the suppression of cancer, ageing, regulation of the cell cycle, apoptosis, and the expression of genes are involved in the transcription factor of the protein P53. The activation of DNA-repairing proteins is enabled by P53 and how it stops the cell cycle at G_1 and G_2. Upon comparison with the control group that detects apoptosis induced by EST, the Bcl2 expressions were substantially elevated in the kidney and liver tissues in the EST group while the apoptotic P53 expression was similarly elevated. Anti-apoptotic effects are implicated within Alanda NPs as the alterations in Bcl2 and P53 expressions are altered by the treatment of Alanda NPs to the EST. Apoptosis can arise after oxidative stress and serious cellular genotoxicity occur due to such cellular and molecular actions. Free radical-induced damage in endothelial cells is safeguarded by natural antioxidants stemming from *E. foeminea* extracts, as per another study[27] that corroborates the results of this work. The findings of this study found that the expressions of P53 and Bcl2 proteins displayed an inverse correlation. Aldubayan et al[10] note bidirectional alterations of protein expression patterns of P53 and Bcl2. Thus, there is potential for apoptosis to take place in the kidney and liver within EST, given the reduction in Bcl2 antiapoptotic cells and the rise in P53 apoptotic cells. A substantial rise in P53 immunoreactivity as a result of the Ehrlich tumor was also observed in another paper[10]. Similarly, heightened P53 expression in the hepatic tissue of mice and diminished liver antioxidant systems are provoked by EAC, per a distinct academic work[50]. Lastly, heightened Bcl2 expression and reduced P53 expression in renal and hepatic tissues were found in EST-carrying mice treated with Alanda NPs, per the results of this study.

Conclusions

Highly safe and efficacious treatments are now embodied by alternative medicine, such as herbal medicine, in the fight against cancer. A novel synthesized nanoparticle design for treatment is presented in this study. A new potential drug to combat cancer could be Alanda NPs extracts, per the promising results discussed. Significantly fewer side effects could result from implementing such new medication, particularly in contrast to chemotherapy.

Data Availability

The data used to support the findings of this study are available from the corresponding author upon request.

Ethics Approval

Our study was approved by the Institutional Animal Care and Use Committee (IACUC – SCI – TU – 0311) and had the capability to underwrite this study, which was guided by the rules provided by the Moral Committee of the Faculty of Science at Tanta University.

Conflicts of Interest

The authors declare that they have no conflicts of interest.

Authors' Contributions

Ehab Tousson, Rehab M. Elgharabawy, Ibrahim E. El Sayed: conception and design of the study; Rehab M. Elgharabawy, Amira S. Ahmed, Doaa T. Gebreel: analysis and interpretation of data; All authors: drafting the article and making critical revisions related to the relevant intellectual content of the manuscript; Rehab M. Elgharabawy, Ehab Tousson: final approval of the version of the article to be published.

ORCID ID

Rehab M. Elgharabawy: 0000-0002-4399-8195
Ehab Tousson: 0000-0001-9722-3603
Ibrahim E. El Sayed: 0000-0002-6418-987
Abd El-Aleim H.: 0000-0002-4625-8651
Mervat Elabd: 0000-0001-5943-8347
Doaa T. Gebreel: 0000-0002-3526-7683

References

1) Tousson E, Hafez E, Zaki S, Gad A. P53, Bcl-2 and CD68 expression in response to amethopterin-induced lung injury and ameliorating role of l-carnitine. Biomed Pharmacother 2014; 68: 631-639.
2) Tousson E, Bayomy MF, Ahmed AA. Rosemary extract modulates fertility potential, DNA fragmentation, injury, KI67 and P53 alterations induced by etoposide in rat testes. Biomed Pharmacother 2018; 98: 769-774.
3) Tousson E, Hafez E, Zaki S, Gad A. The cardioprotective effects of L-carnitine on rat cardiac injury, apoptosis, and oxidative stress caused by amethopterin. Environ Sci Pollut Res 2016; 23: 20600-20608.
4) Mutar TF, Tousson E, Hafez E, Abo Gazia M, Salem SB. Ameliorative effects of vitamin B17 on the kidney against Ehrlich ascites carcinoma induced renal toxicity in mice. Environ Toxicol 2020; 35: 528-537.
5) Tousson E, Hafez E, Zaki S, Gad A, Elgharabawy RM. Evaluation of the testicular protection conferred by damiana (Turnera diffusa Willd.) against amitriptyline-induced testicular toxicity, DNA damage and apoptosis in rats. Biomed Pharmacother 2020; 132: 110819.
6) Alotaibi B, Tousson E, El-Masry TA, Altwaijry N, Saleh A. Ehrlich ascites carcinoma as model for studying the cardiac protective effects of curcumin nanoparticles against cardiac damage in female mice. Environ Toxicol 2021; 36: 105-113.
7) Abdelbasset WK, Ibrahim AA, Alsubaie SF, Alrawaili SM, Althomali OW, Hussein HM, Sulieman A, Kanwal R. Awareness and knowledge of breast cancer rehabilitation among Saudi Arabia physical therapists. Eur Rev Med Pharmacol Sci 2023; 27: 5370-5377.
8) Elgharabawy RM, El Tantawy El Sayed I, Abd-Allah Rezk N, Tousson E. Therapeutic Impact of Costus (Saussurea lappa) Against Ehrlich Solid Tumor-Induced Cardiac Toxicity and DNA Damage in Female Mice. Front Pharmacol 2021; 12: 708785.
9) Oshiba RT, Touson E, Elsherbini YM, Abdraboh ME. Melatonin: A regulator of the interplay between FoxO1, miR96, and miR215 signaling to diminish the growth, survival, and metastasis of murine adenocarcinoma. BioFactors 2021; 47: 740-753.
10) Aldubayan MA, Elgharabawy RM, Ahmed AS, Tousson E. Antineoplastic activity and curative role of avenanthramides against the growth of ehrlich solid tumors in mice. Oxid Med. Cell Longev 2019; 2019: 5162687.
11) El-Masry TA, Al-Shaalan NH, Tousson E, Buabeid M, Alyousef AM. The therapeutic and antineoplastic effects of vitamin B17 against the growth of solid-form Ehrlich tumours and the associated changes in oxidative stress, DNA damage, apoptosis and proliferation in mice. Pak J Pharm Sci 2019; 32: 2801-2810.
12) El-Masry T, Al-Shaalan N, Tousson E, Buabeid M, Al-Ghadeer A. Potential therapy of vitamin B17 against Ehrlich solid tumor induced changes in Interferon gamma, Nuclear factor kappa B, DNA fragmentation, p53, Bcl2, survivin, VEGF and TNF-α Expressions in mice. Pak J Pharm Sci 2020; 33: 393-401.
13) Abd Eldaim MA, Tousson E, El Sayed IE, Abd El AE, Elsharkawy HN. Grape seeds proanthocyanidin extract ameliorates Ehrlich solid tumor induced renal tissue and DNA damage in mice. Biomed Pharmacother 2019; 115: 108908.
14) Abd Eldaim MA, Tousson E, El Sayed IE, Abd Elmaksoud AZ, Ahmed AA. Ameliorative effects of 9-diaminoacridine derivative against Ehrlich ascites carcinoma–induced hepatorenal injury in mice. Environ Sci Pollut Res 2021; 28: 21835-21850.
15) Abd Eldaim MA, Tousson E, Soliman MM, El Sayed IE, Aleem AA, Elsharkawy HN. Grape seed extract ameliorated Ehrlich solid tumor-induced hepatic tissue and DNA damage with reduction of PCNA and P53 protein expression in mice. Environ Sci Pollut Res 2021; 28: 44226-44238.
16) Elgharabawy RM, Alhowail AH, Emara AM, Aldubayan MA, Ahmed AS. The impact of chicory (Cichoriumintybus L.) on hemodynamic functions and oxidative stress in cardiac toxicity induced by lead oxide nanoparticles in male rats. Biomed Pharmacother 2021; 137: 111324.
17) Al Garea MH, Alqasoumi AA, Alqahtani SA, Hadadi AH, Emara AM. Vitamin C as a potential ameliorating agent against hepatotoxicity among alcoholic abusers. Eur Rev Med Pharmacol Sci 2023; 27: 3322-3335.
18) 18 Moustafa AH, Ali EM, Moselhey SS, Tousson E, El-Said KS. Effect of coriander on thioacetamide-induced hepatotoxicity in rats. Toxicol Ind Health 2014; 30: 621-629.
19) 19 Alhowail A, Chigurupati S, Elgharabawy R, Aldubayan M. Co-administration of imipramine and doxorubicin reduces the survival rate and body weight of mice. Eur Rev Med Pharmacol Sci 2020; 24: 12978-12982.
20) El-Gharieb MA, El-Masry TA, Emara AM, Hashem MA. Potential hepatoprotective effects of vitamin E and Nigella sativa oil on hepatotoxicity induced by chronic exposure to malathion in human and male albino rats. Toxicol Environ Chem 2010; 92: 391-407.
21) Mighri H, Akrout A, Bennour N, Eljeni H, Zammouri T, Neffati M. LC/MS method development for the determination of the phenolic compounds of Tunisian Ephedra alata hydromethanolic extract and its fractions and evaluation of their antioxidant activities. S Afr J Bot 2019; 124: 102-110.
22) Chouikh A. Phytochemical profile, antioxidant, analgesic and hypolipidaemic effects of ephedra alata decne. female cones extract. Farmacia 2020; 68: 1011-1020.
23) Krizevski R, Bar E, Shalit O, Sitrit Y, Ben-Shabat S, Lewinsohn E. Composition and stereochemistry of ephedrine alkaloids accumulation in Ephedra sinica Stapf. Phytochem 2010; 71: 895-903.
24) Elhadef K, Smaoui S, Fourati M, Ben Hlima H, Chakchouk Mtibaa A, Sellem I, Ennouri K, Mel-

louli L. A review on worldwide Ephedra history and story: from fossils to natural products mass spectroscopy characterization and biopharmacotherapy potential. Evid. Based Complement Alternat Med 2020; 2020: 1540638.

25) Roh JS, Lee H, Lim J, Kim J, Yang H, Yoon Y, Shin SS, Yoon M. Effect of Gangjihwan on hepatic steatosis and inflammation in high fat diet-fed mice. J Ethnopharmacol 2017; 206: 315-326.

26) Soumaya B, Yosra E, Rim BM, Sarra D, Sawsen S, Sarra B, Kamel M, Wissem AW, Isoda H, Wided MK. Preliminary phytochemical analysis, antioxidant, anti-inflammatory and anticancer activities of two Tunisian ephedra species: Ephedra alata and Ephedra fragilis. S Afr J Bot 2020; 135: 421-428.

27) Khalil M, Khalifeh H, Saad F, Serale N, Salis A, Damonte G, Lupidi G, Daher A, Vergani L. Protective effects of extracts from Ephedra foeminea Forssk fruits against oxidative injury in human endothelial cells. J Ethnopharmacol 2020; 260: 112976.

28) Dbeibia A, Taheur FB, Altammar KA, Haddaji N, Mahdhi A, Amri Z, Mzoughi R, Jabeur C. Control of Staphylococcus aureus methicillin resistant isolated from auricular infections using aqueous and methanolic extracts of Ephedra Alata. Saudi J Biol Sci 2022; 29: 1021-1028.

29) Danciu C, Muntean D, Alexa E, Farcas C, Oprean C, Zupko I, Bor A, Minda D, Proks M, Buda V, Hancianu M. Phytochemical characterization and evaluation of the antimicrobial, antiproliferative and pro-apoptotic potential of Ephedra alata Decne. hydroalcoholic extract against the MCF-7 breast cancer cell line. Mol 2018; 24: 13.

30) Mendelovich M, Shoshan M, Fridlender M, Mazuz M, Namder D, Nallathambi R, Selvaraj G, Kumari P, Ion A, Wininger S, Nasser A. Effect of Ephedra foeminea active compounds on cell viability and actin structures in cancer cell lines. J Med Plant Res 2017; 11: 690-702.

31) Jaradat NA, Shawahna R, Eid AM, Al-Ramahi R, Asma MK, Zaid AN. Herbal remedies use by breast cancer patients in the West Bank of Palestine. J Ethnopharmacol 6; 178: 1-8.

32) Zhao Z, Han J, Xu S, Jin Z, Yin TH, Zhao K. Amoxicillin encapsulated in the N-2-hydroxypropyl trimethyl ammonium chloride chitosan and N, O-carboxymethyl chitosan nanoparticles: Preparation, characterization, and antibacterial activity. Int J Biol Macromol 2022; 221: 613-622.

33) Mittal N, Kaur G. Investigations on polymeric nanoparticles for ocular delivery. Adv Polym Technol 2019; 2019: 1316249.

34) Neeraj NS, Mordina B, Srivastava AK, Mukhopadhyay K, Prasad NE. Impact of process conditions on the electrochemical performances of NiMoO4 nanorods and activated carbon based asymmetric supercapacitor. Appl Surf Sci 2019; 473: 807-819.

35) Mellado M, Soto M, Madrid A, Montenegro I, Jara-Gutiérrez C, Villena J, Werner E, Godoy P, Aguilar LF. In vitro antioxidant and antiproliferative effect of the extracts of Ephedra chilensis K Presl aerial parts. BMC Complement Altern Med 2019; 19: 1-10.

36) Madani F, Esnaashari SS, Mujokoro B, Dorkoosh F, Khosravani M, Adabi M. Investigation of effective parameters on size of paclitaxel loaded PLGA nanoparticles. Adv Pharm Bull 2018; 8: 77.

38) Reitman S, Frankel S. A colorimetric method for the determination of serum glutamic oxalacetic and glutamic pyruvic transaminases. Am J Clin Pathol 1957; 28: 56-63.

39) Doumas BT, Watson WA, Biggs HG. Albumin standards and the measurement of serum albumin with bromcresol green. Clin Chim Acta 1971; 31: 87-96.

40) Emara AM, Alrasheedi KA, Aldubayan MA, Alhowail AH, Elgarabawy RM. Effect of inhaled waste anaesthetic gas on blood and liver parameters among hospital staff. Hum Exp Toxicol 2020; 39: 1585-1595.

41) Saggu S, Sakeran MI, Zidan N, Tousson E, Mohan A, Rehman H. Ameliorating effect of chicory (Chichorium intybus L.) fruit extract against 4-tertoctylphenol induced liver injury and oxidative stress in male rats. Food and Chem Toxicol 2014; 72: 138-141.

42) Bowers LD, Wong ET. Kinetic serum creatinine assays. II. A critical evaluation and review. Clin Chem 1980; 26: 555-561.

43) Elmasry TA, Al-Shaalan NH, Tousson E, El-Morshedy K, Al-Ghadeer A. Star anise extracts modulation of reproductive parameters, fertility potential and DNA fragmentation induced by growth promoter Equigan in rat testes. Braz J Pharm Sci 2018; 54: 1-10.

44) Labarca C, Paigen K. A simple, rapid, and sensitive DNA assay procedure. Anal Biochem 1980; 102: 344-352.

45) Tousson E. Histopathological alterations after a growth promoter boldenone injection in rabbits. Toxicol Ind Health 2016; 32: 299-305.

46) Kabel AM, Abdel-Rahman MN, El-Sisi AEDE. Effect of atorvastatin and methotrexate on solid Ehrlich tumor. Eur J Pharmacol 2013; 713: 47-53.

47) Badr OM, Sakr S, Abd-Eltawab HA. Ameliorative effect of ginger extract against pathological alterations induced in mice bearing solid tumors. J Biosci Appl Res 2016; 2: 185-196.

48) Salama AF, Kasem SM, Tousson E, Elsisy MK. Protective role of L-carnitine and vitamin E on the kidney of atherosclerotic rats. Biomed Aging Pathol 2012; 2: 212-215.

49) Al-Rasheed NM, El-Masry TA, Tousson E, Hassan HM, Al-Ghadeer A. Hepatic protective effect of grape seed proanthocyanidin extract against Gleevec-induced apoptosis, liver Injury and Ki67 alterations in rats. Braz J Pharm Sci 2018; 54: e17391.

50) Alapati V, Noolvi MN, Manjula SN, Pallavi KJ, Patel HM, Tippeswamy BS, Satyanarayana SV. In vivo anti-tumour activity of novel Quinazoline derivatives. Eur Rev Med Pharmacol Sci 2012; 16: 1753-1764.